Supporting Information for

Optically and electrically excited intermediate electronic states in donor:acceptor based OLEDs

Nikolai Bunzmann[1], Sebastian Weissenseel[1], Liudmila Kudriashova[1], Jeannine Gruene[1], Benjamin Krugmann[1], Juozas Vidas Grazulevicius[2], Andreas Sperlich[1*] and Vladimir Dyakonov[1,3]

[1] Experimental Physics VI, Julius Maximilian University of Würzburg, 97074 Würzburg, Germany
[2] Department of Polymer Chemistry and Technology at Kaunas University of Technology, Radvilenu pl. 19, LT-50254 Kaunas, Lithuania

(Dated: January 3, 2020)
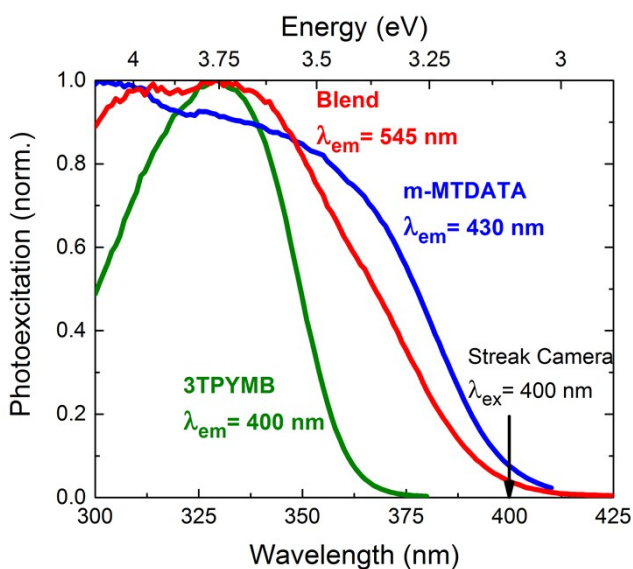
FIG. S1. Photoexcitation spectra of solid films of m-MTDATA, 3TPYMB and their blend. Excitation with a 400 nm laser in the streak camera measurements, or with a 365 nm UV LED in PLDMR will only excite m-MTDATA, but not 3TPYMB.
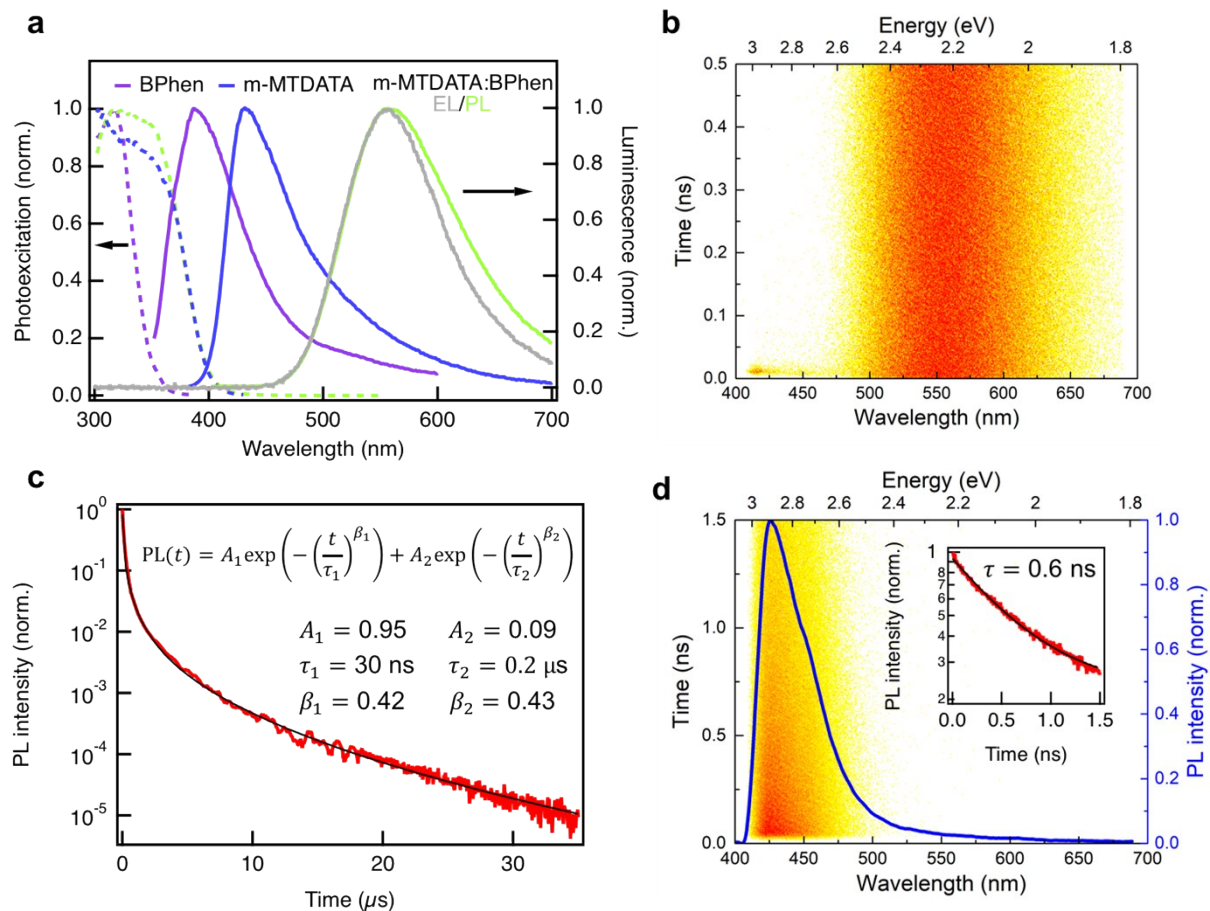
FIG. S2. Photophysics of m-MTDATA:BPhen. **a)** PE and PL spectra of solid films of BPhen, m-MTDATA and their blend together with an EL spectrum of an OLED based on m-MTDATA:BPhen. **b)** Streak camera image of PL from an m-MTDATA:BPhen blended solid film for excitation at $\lambda_{exc} = 400$ nm. **c)** Transient PL decay of an m-MTDATA:BPhen blended solid film. A sum of two stretched exponential decays was used to fit the curve and the resulting parameters are listed in the inset. Note that the characteristic lifetimes obtained from the stretched exponential decay do not necessarily represent the lifetimes of prompt and delayed fluorescence. **d)** Streak camera image of PL from a solid film of pristine m-MTDATA. Inset: PL decay curve of this emission. A lifetime of 0.6 ns is obtained from fitting the transient with a single exponential decay.
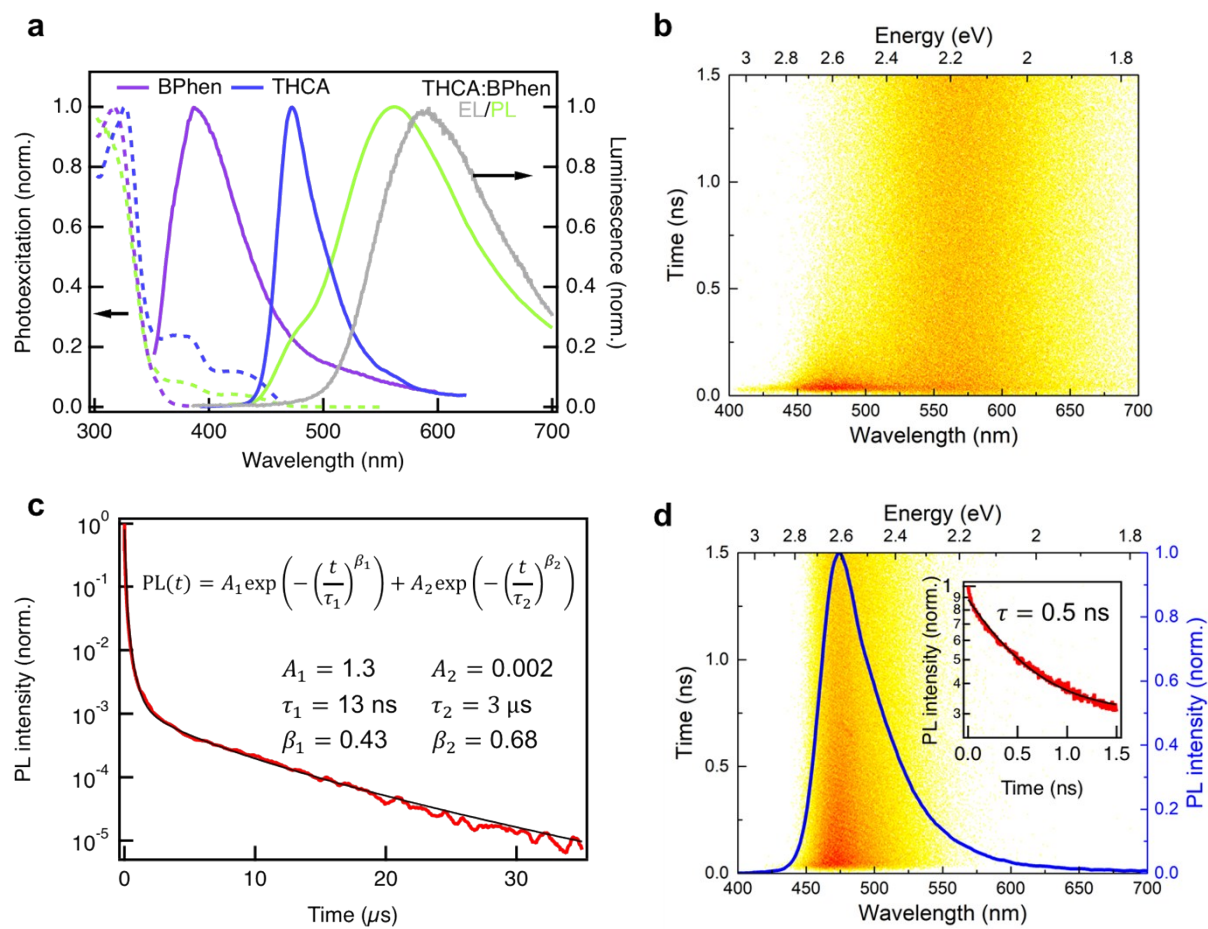
FIG. S3. Photophysics of THCA:BPhen. **a)** PE and PL spectra of solid films of BPhen, THCA and their blend together with an EL spectrum of a bilayer OLED based on THCA:BPhen. **b)** Streak camera image of PL from a THCA:BPhen blended solid film for excitation at $\lambda_{exc} = 400$ nm. **c)** Transient PL decay of a THCA:BPhen blended solid film. A sum of two stretched exponential decays was used to fit the curve and the resulting parameters are listed in the inset. Note that the characteristic lifetimes obtained from the stretched exponential decay do not necessarily represent the lifetimes of prompt and delayed fluorescence. **d)** Streak camera image of PL from a solid film of pristine THCA. Inset: PL decay curve of this emission. A lifetime of 0.5 ns is obtained from fitting the transient with a single exponential decay.

In figure c:

$$\mathrm{PL}(t) = A_1 \exp\left(-\left(\frac{t}{\tau_1}\right)^{\beta_1}\right) + A_2 \exp\left(-\left(\frac{t}{\tau_2}\right)^{\beta_2}\right)$$

$A_1 = 1.3$ $A_2 = 0.002$
$\tau_1 = 13$ ns $\tau_2 = 3$ μs
$\beta_1 = 0.43$ $\beta_2 = 0.68$

In figure d inset: $\tau = 0.5$ ns
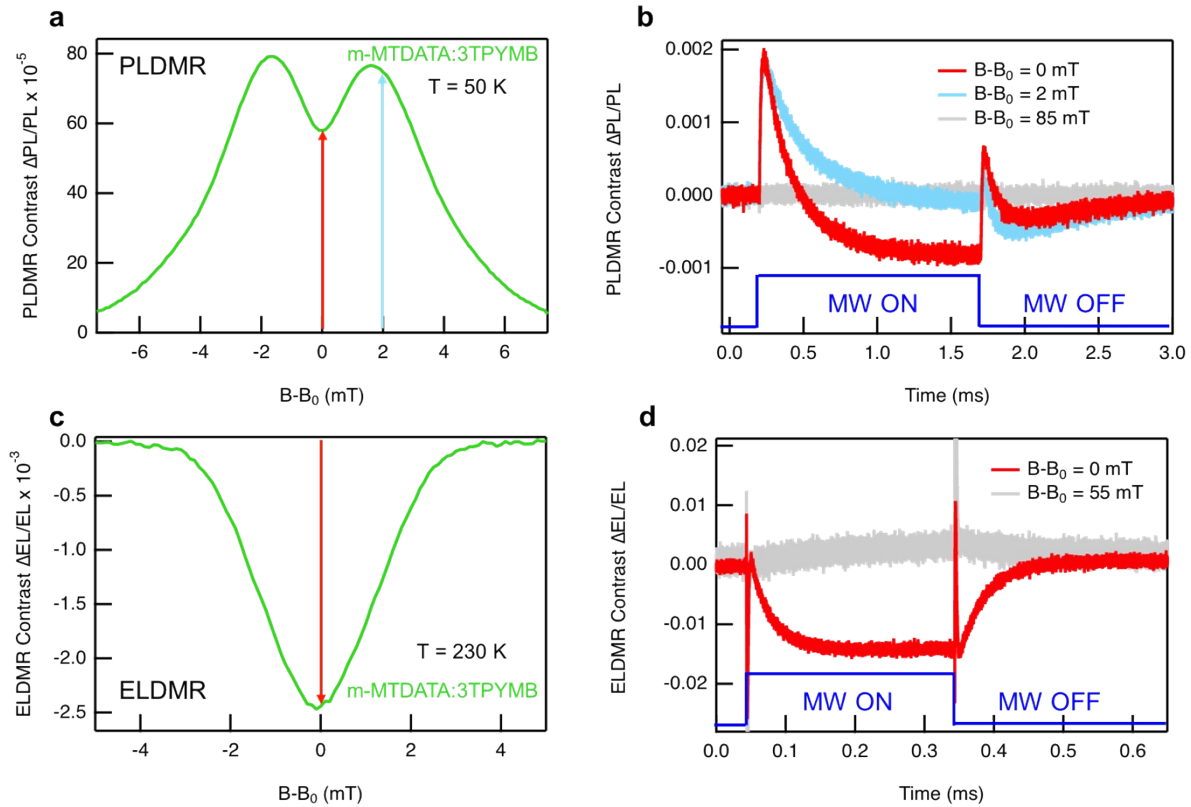
FIG. S4. Comparison of lock-in and directly measured PLDMR and ELDMR signals **a)** Lock-in detected PLDMR signal of an m-MTDATA:3TPYMB blend at 50 K. **b)** Transient measurement of the microwave induced change of PL at a constant external magnetic field. The time-dependent change of PL is measured at different magnetic field positions of the PLDMR spectrum (Graph **a**), as indicated by the arrows. **c)** Lock-in detected ELDMR signal of an OLED based on m-MTDATA:3TPYMB at 230 K. **d)** Transient measurement of the microwave induced change of EL at a constant external magnetic field. The time-dependent change of EL is measured at a magnetic field position in resonance which is indicated by an arrow in the graph of the lock-in detected ELDMR signal (Graph **c**). The off-resonance measurements (gray), which determines the baseline, and the on-off microwave modulation sequences (blue) are also shown.

In order to determine the sign of PLDMR and ELDMR signals we used an oscilloscope to monitor the time dependent microwave induced change in PL/EL during microwave on-off modulation at a constant magnetic field.

For PLDMR, transients at three different magnetic field positions are measured. For the first measurement the magnetic field is set to $B-B_0 = 0$ mT where narrow and broad component are superimposed in the lock-in detected signal (**Fig. S4a**, red arrow). The time trace measured with the oscilloscope exhibits a rapid increase of PL, when resonant microwaves are switched on, which decays over time afterwards (**Fig. S4b**, red curve). The intensity does not decay back to the initial PL intensity but there is an additional negative offset. In a second measurement the magnetic field is set to $B-B_0 = 2$ mT where only the broad signal is in resonance (**Fig. S4a**, blue arrow). Here the time trace measured with the oscilloscope exhibits a rapid increase of PL but in this case the intensity decays back to its initial intensity (**Fig. S4b**, blue curve). Finally, a third measurement at $B-B_0 = 85$ mT shows that there is no off-resonance microwave induced change of PL (**Fig. S4b**, grey curve). From the difference between time traces at $B-B_0 = 0$ mT and $B-B_0 = 2$ mT we conclude that the rapid increase is attributed to the broad lock-in detected component and the negative offset to the narrow component. Furthermore, these measurements reveal that the broad component corresponds to an increase of PL intensity and the narrow component to a decrease. Based on these findings we are now able to set the sign of the superimposed signal components in lock-in detected PLDMR measurements with certainty: narrow components exhibit a negative sign while broad components exhibit a positive sign.

For ELDMR, transients at two different magnetic field positions are measured. For the first measurement the magnetic field is set to $B-B_0 = 0$ mT where the resonance condition is fulfilled (**Fig. S4c**, red arrow). The corresponding time trace measured with the oscilloscope exhibits a decay of EL intensity when resonant microwaves are switched on (**Fig. S4d**, red curve). This decay saturates at a level below the initial EL intensity.

From this measurement we conclude that the microwave induce change of EL in resonance corresponds to a decrease of EL intensity. Therefore, we set the sign in lock-in detected ELDMR measurements to negative.

The effect of static magnetic field on EL intensity (magneto-electroluminesence, MEL) (Fig. S5) confirms the built-up of spin polarisation of triplet exciplex state in magnetic field due to different lifetimes of the triplet Zeeman sublevels m_S=0, +/-1.
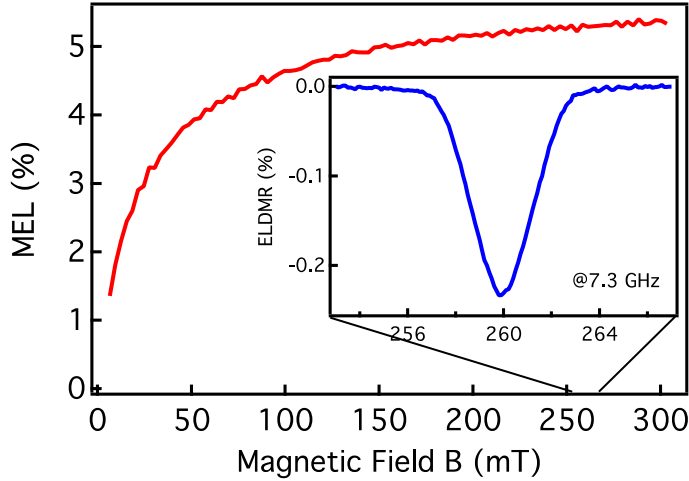
FIG. S5. Magnetic field effect on electroluminescence (MEL) in an OLED based on m-MTDATA:3TPYMB at T= 220 K. EL enhancement is measured directly. Inset: Separately measured ELDMR on the same device with 7.3 GHz on/off modulated microwaves and lock-in phase-sensitive detection. The sign of ELDMR is directly determined from the transient EL measurements as in **Fig. S4d**.
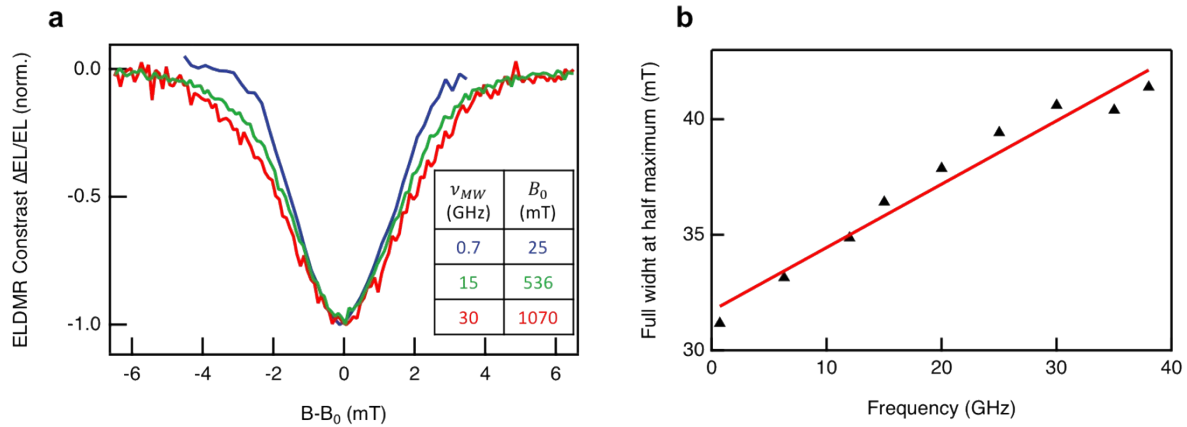
FIG. S6. **a)** Normalized ELDMR spectra of m-MTDATA:3TPYMB based OLEDs at different microwave frequencies ν_{MW} and magnetic fields B_0. The magnetic field axis is shifted, such that resonance peaks at B_0 are centred around $B - B_0$. The temperature for all measurements was T = 230 K. **b)** Frequency dependence of the full width at half maximum of ELDMR spectra.

The microwave frequency dependence of the linewidth of ELDMR spectra can be used to estimate the difference Δg in g-factors of electron and hole forming the exciplex state. The following considerations explain the theoretical background of this method.
Under magnetic resonance conditions the following equation is fulfilled:

$$h\nu_{MW} = g\mu_B B\Delta m_s \tag{S1}$$

5

Here ν_{MW} is the microwave frequency, h is the Planck constant, g is the g-factor of the spin, μ_B is the Bohr magneton, B is the magnetic field value and $\Delta m_s = 1$ is the allowed change of the magnetic quantum number. For two independent spins with g-factors g_a and g_b (in the case of an exciplex state these two spins correspond to electron and hole spin located on separate molecules) the difference ΔB of the resonance positions of the two spins on the magnetic field axis is given by:

$$\Delta B = \left(\frac{1}{g_a} - \frac{1}{g_b} \right) \frac{h\nu_{MW}}{\mu_B} \qquad (S2)$$

According to equation S2 the magnetic field splitting ΔB depends linearly on the microwave frequency ν_{MW} if $\Delta g = |g_a - g_b| > 0$. At low frequencies, ΔB is negligible and the resonance curves of the two spins overlap. In this case the linewidth of the overall EPR signal is dominated by broadening mechanisms such as dipolar interaction D and unresolved hyperfine interactions. For higher microwave frequencies the increase of ΔB causes an additional broadening of the EPR linewidth as shown in Figure S6.

The resonant transmission line approach we use to measure ELDMR spectra (see experimental section and **Fig. S17**) allows us to measure at different microwave frequencies and probe the above described behavior. We were able to measure ELDMR spectra in a frequency range between 0.7 and 38 GHz. Exemplary spectra for 0.7, 15 and 30 GHz are shown in **Fig. S6a**. Here, an increase of the linewidth for higher frequencies can be observed. Evaluation of the frequency dependence of the full width at half maximum for all ELDMR spectra in the frequency range between 0.7 and 38 GHz shows a roughly linear dependence as depicted in **Fig. S6b**. This observation is in line with equation S2 and indicates $\Delta g > 0$.

An upper boundary value for Δg can be extracted from a simulation of the ELDMR spectra within the whole frequency range. For this purpose we used the software package EasySpin,[1] which is commonly used to extract parameters from EPR spectra. Here, a system of two coupled spins with different g-factors was assumed. Every spectrum in the accessible frequency range was included in a global fit. We use $\bar{g} = (g_a + g_b)/2$ as the mean g-factor and $\Delta g = |g_a - g_b|$ as the difference in fixed, scalar g-factors. Alternatively, anisotropy (g-tensor) or a possible distribution of exciplexes with slightly different g-factors (g-strain) would also result in a magnetic field-dependent broadening. This can be caused by the flexibility of the involved molecules, as well as by the undefined geometry of interacting donor and acceptor molecules hosting an exciplex. These possibilities cannot be discerned with this data set alone, as no actual splitting of the resonance spectrum is observed that would directly indicate Δg as described in equation S2. The choice for this preliminary analysis to fit with fixed g-factors and leaving out g anisotropy and g strain still yields an upper limit for the value of Δg. Yet, this limit embraces any actual g-tensor strain or anisotropy. From our dataset we obtain $\Delta g < 9.2 \cdot 10^{-4}$. The value of the mean g-factor $\bar{g} = 2.0007$ is close to the g-factor of a free electron and typical for polarons in organic semiconductors. We are not able to assign separate values to the electron and hole but rather can only determine the difference between them.

The fit is performed using EasySpin - a software toolbox based on Matlab, which simulates EPR spectra of spin systems. The starting parameters for the fit are defined as follows:

```
Sys.S=[1/2 1/2];  %specifies the system as two spin ½ carrying particles.
Sys.g = [2.00118 ; 2.00021];  %sets the initial values for the g-factors of the two spins.
Sys.D=[27];  %sets the initial value for the dipolar interaction to 27 MHz.
Sys.lw=4;  %sets the initial value for the Gaussian broadening of the linewidth to 4 mT.
```

First, the spin system is defined as two spin ½ particles with corresponding g-factors, which, in our case, represent electron and hole forming an exciplex state. Furthermore, a dipolar coupling D between the two spins is defined. D basically contains information about the distance of the two spins as described in the main part of this work. An initial linewidth for the EPR spectrum has to be set to account for broadening mechanisms such as unresolved hyperfine coupling. On the one hand, EasySpin allows to *simulate* a theoretical EPR spectrum of such a spin system if the user provides the values for the g-factors, the dipolar coupling and the initial linewidth as well as the frequency at which the EPR experiment is performed. On the other hand, EasySpin can be used to *fit* experimental data, where the parameters of the spin system are optimized to reproduce the measured signal. For a global fit this optimization is performed for several spectra simultaneously. General Information on EasySpin can be found in [1] or at easyspin.org/easyspin/documentation/
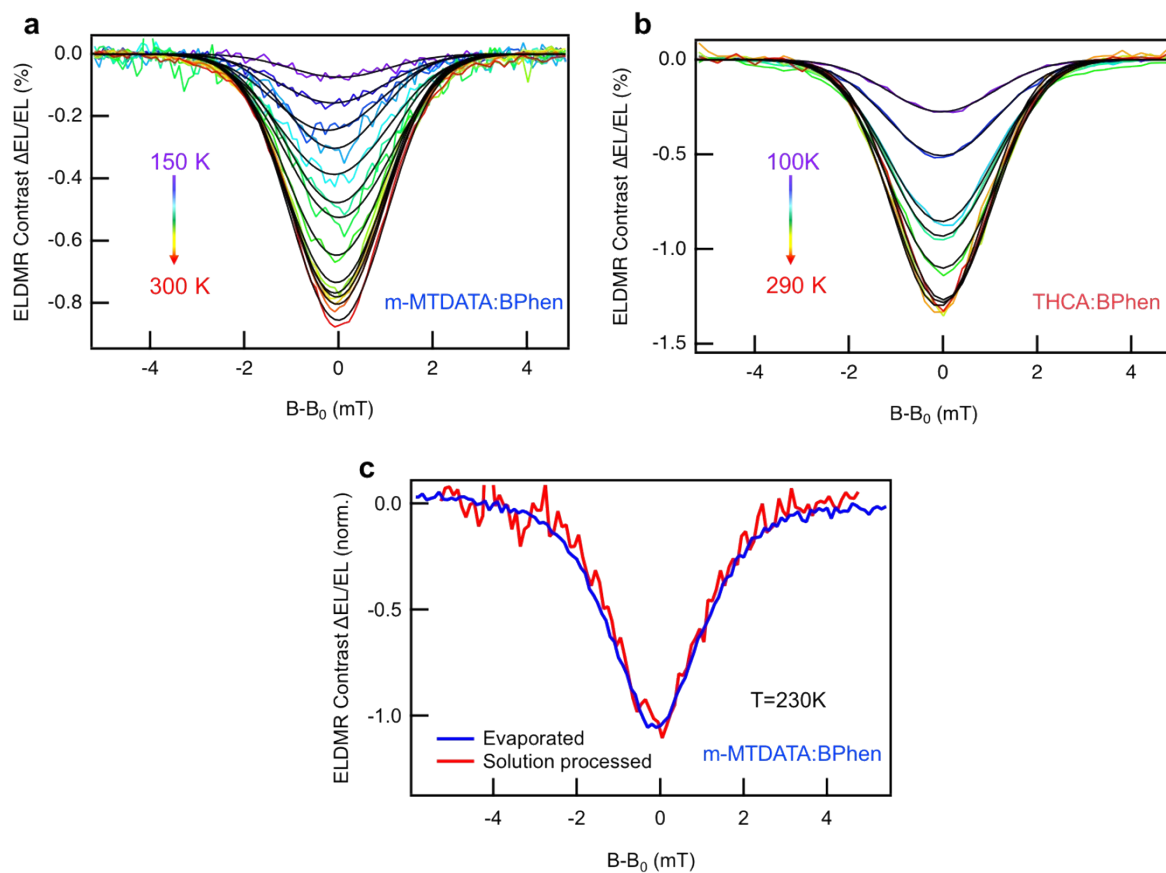
FIG. S7. Temperature-dependent ELDMR of **a)** m-MTDATA:BPhen and **b)** THCA:BPhen together with Gaussian fits (black lines). For both material combinations the signal decreases with decreasing temperature, which is in agreement with TADF behaviour. **c)** Normalized ELDMR spectra measured on m-MTDATA:BPhen OLEDs based either on evaporated donor and acceptor (blue), or solution processed donor and evaporated acceptor. Spectra are nearly identical showing that the ELDMR signal does not depend on the preparation method.
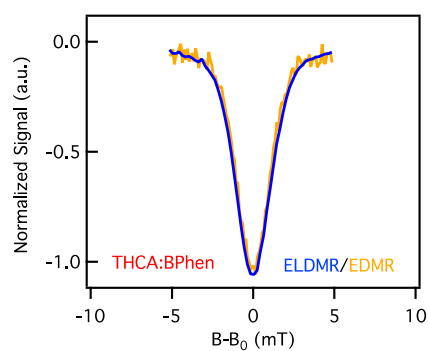
FIG. S8. Normalized ELDMR and EDMR spectra for THCA:BPhen. Both methods yield signals with identical shape, therefore originating from the same effect. We assume the enhanced recombination of exciplexes in resonance (ELDMR) induces a change of the current (EDMR) .
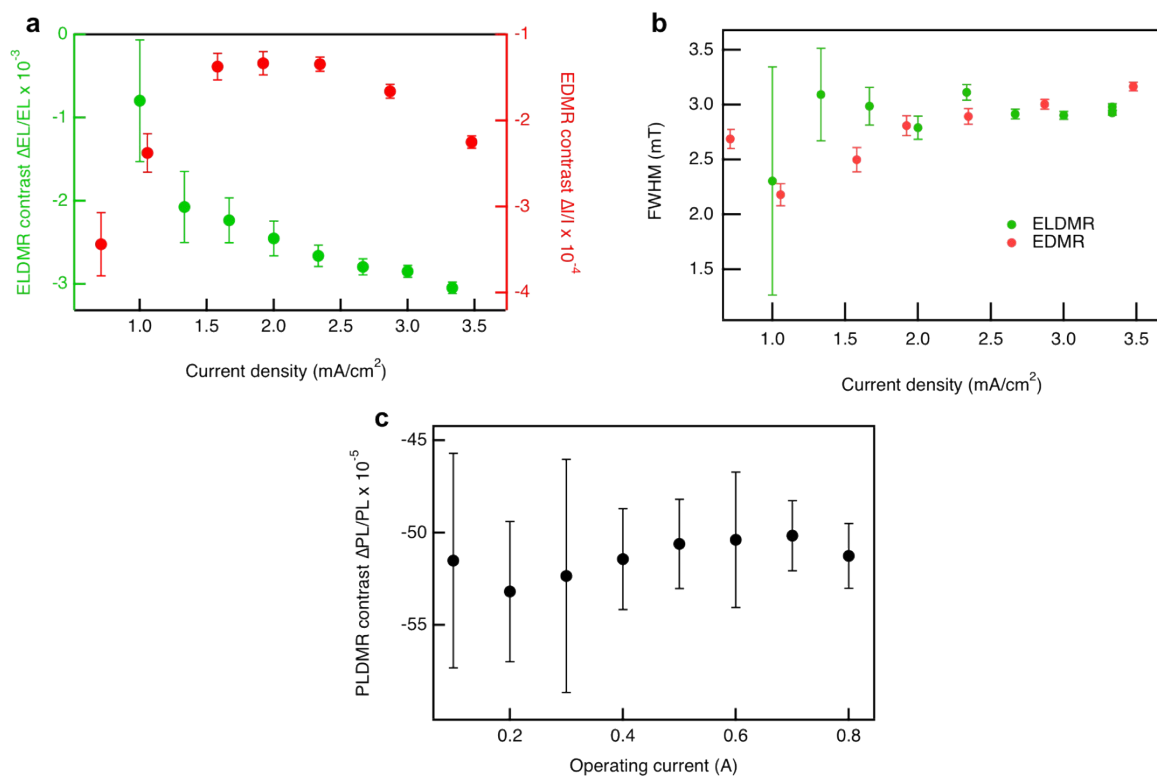
FIG. S9. Dependence of the signal intensities of magnetic resonance measurements on excitation power for m-MTDATA:3TPYMB. **a)** Dependence of ELDMR and EDMR signal intensities on the current density in the OLED at T=220 K. **b)** Dependence of the full width at half maximum (FWHM) in EDMR and ELDMR on the current density in an OLED at T=220 K. **c)** Dependence of PLDMR signal intensities on the excitation power at T=RT. A UV LED is used for optical excitation in PLDMR measurements. Note, the power output of the UV LED is proportional to the operating current that is why the x-axis can be treated as excitation power.
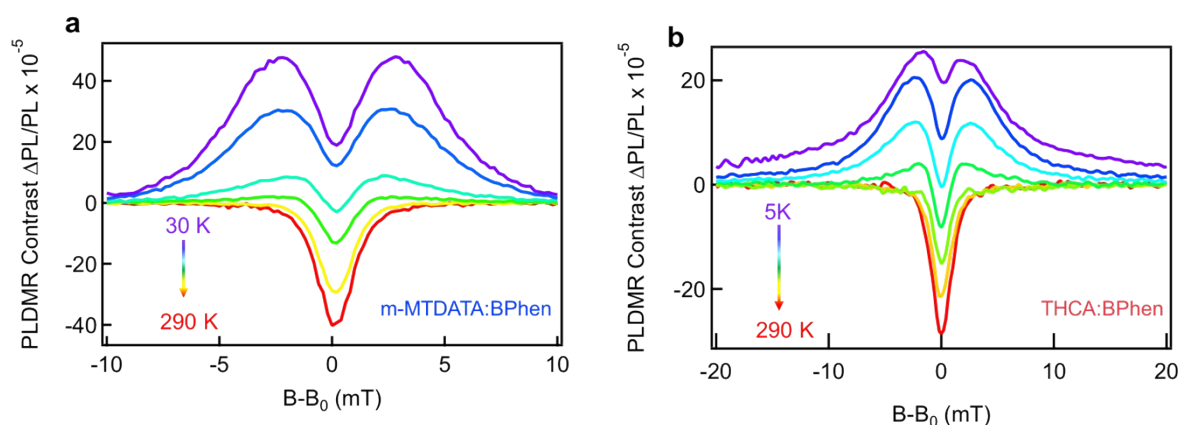
FIG. S10. Temperature dependent PLDMR spectra for the donor:acceptor blends **a)** m-MTDATA:BPhen and **b)** THCA:BPhen. In both molecular blends, the PLDMR spectrum consists of a narrow signal which dominates at room temperature and an additional broad signal which is more pronounced at low temperatures. The narrow (negative) signal is assigned to the exciplex triplet and the broad (positive) signal to the local triplet exciton of the respective donor molecule.
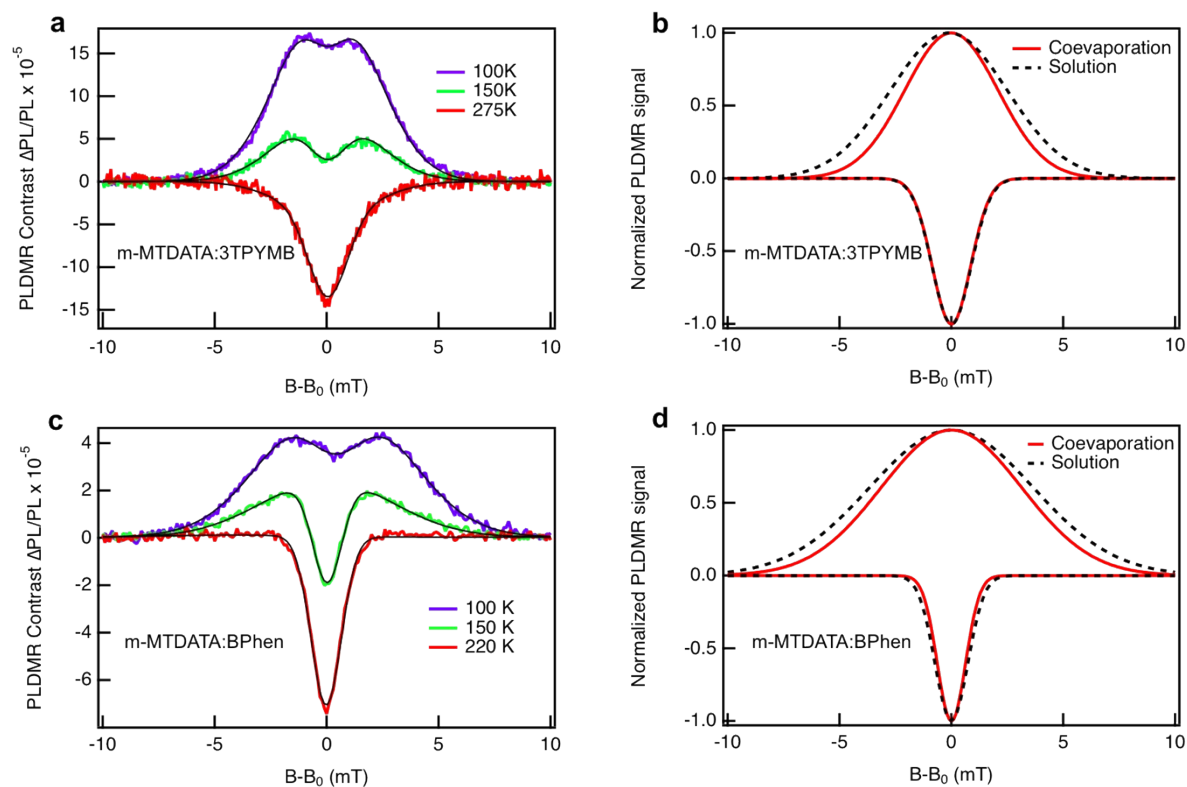
FIG. S11. **a)** Temperature dependent PLDMR measurements on a coevaporated m-MTDATA:3TPYMB sample. The signal shape and temperature behaviour are very similar to those measured on solution processed solid films shown in **Fig. 4b** in the main text. **b)** Normalized fit components obtained for solution processed solid films and evaporated m-MTDATA:3TPYMB samples. **c)** Temperature dependent PLDMR measurements on a coevaporated m-MTDATA:BPhen sample. **d)** Normalized fit components obtained on solution processed solid films and evaporated m-MTDATA:BPhen samples. In both molecular systems, the narrow components (exciplex states) are identical, whereas the broad components are slightly narrower in the vacuum processed solid films, which can be attributed to a larger radius of molecular triplet excitons in the latter.
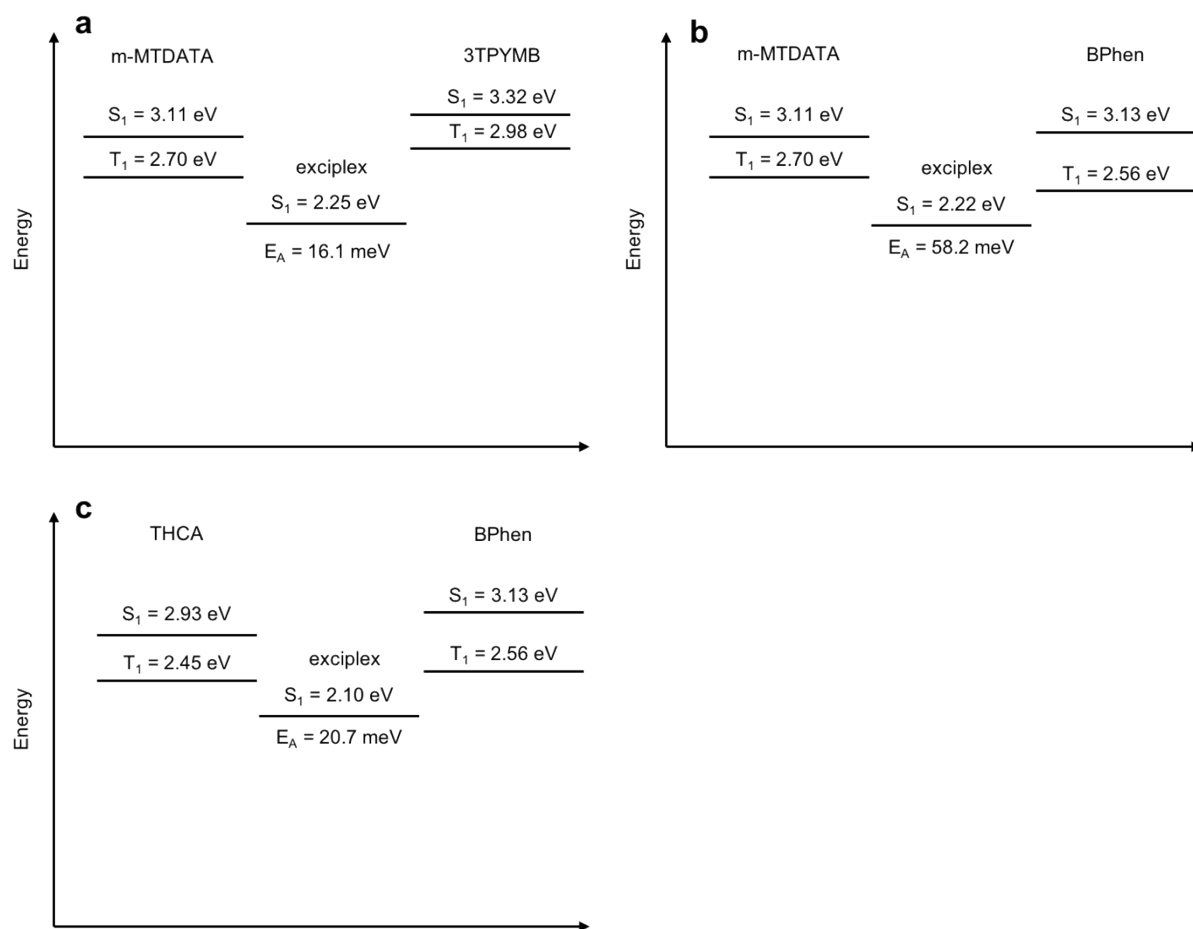
FIG. S12. Energy diagrams showing singlet and triplet energies of individual donor and acceptor molecules as well as of the exciplex state formed at the respective interfaces. **a)** m-MTDATA:3TPYMB **b)** m-MTDATA:BPhen **c)** THCA:BPhen. Values for singlet and triplet states of m-MTDATA and 3TPYMB are taken from [2], for BPhen from [3] and for THCA from [4]. Values for the exciplex states were calculated from peaks of PL spectra for each donor:acceptor combination. (**Fig. 1**, **Fig. S2, Fig. S3**) The activation energies are derived from the Arrhenius plot in **Fig. 3c**.
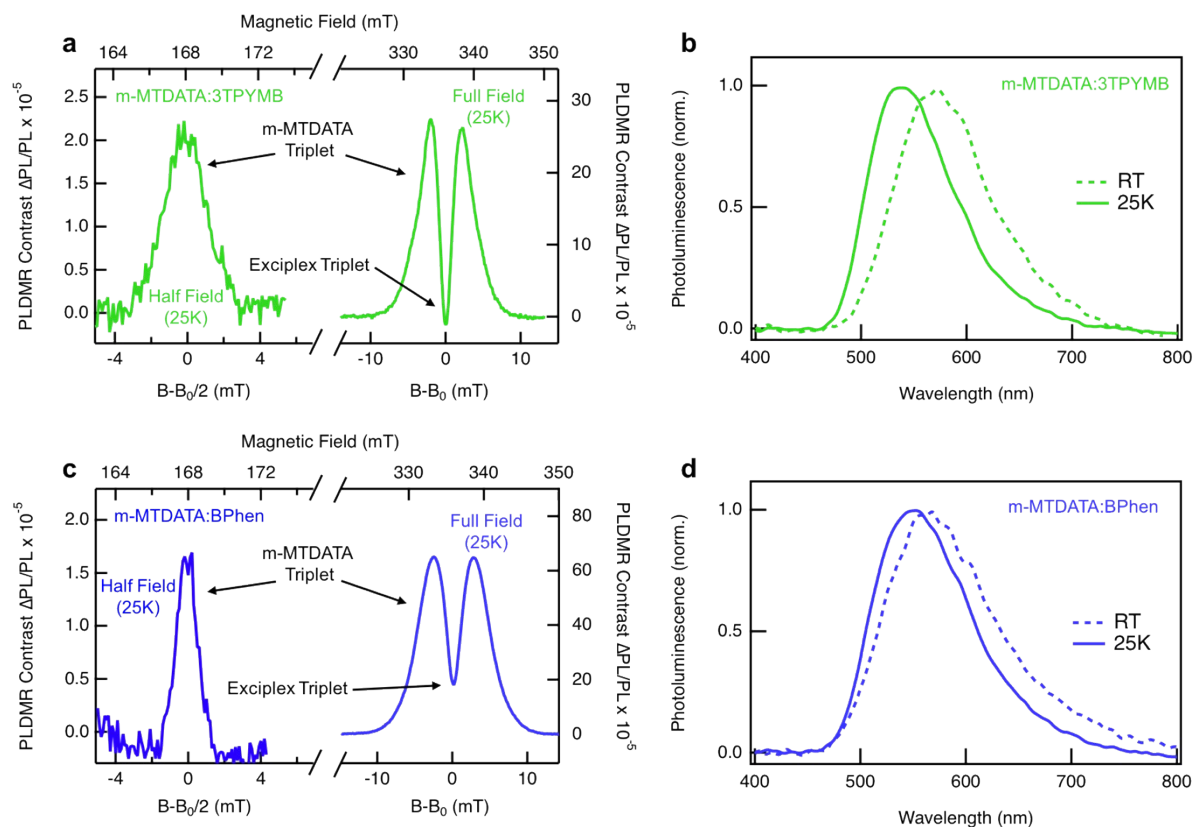
FIG. S13. Half-field and full-field PLDMR signals in **a)** m-MTDATA:3TPYMB and **c)** m-MTDATA:BPhen blends. T=25 K. PL spectra from **b)** m-MTDATA:3TPYMB and **d)** m-MTDATA:BPhen blends recorded at T=25 K (solid lines) and RT (dashed lines). In this temperature range, only PL from the exciplex singlet state is visible exhibiting a small blue shift.
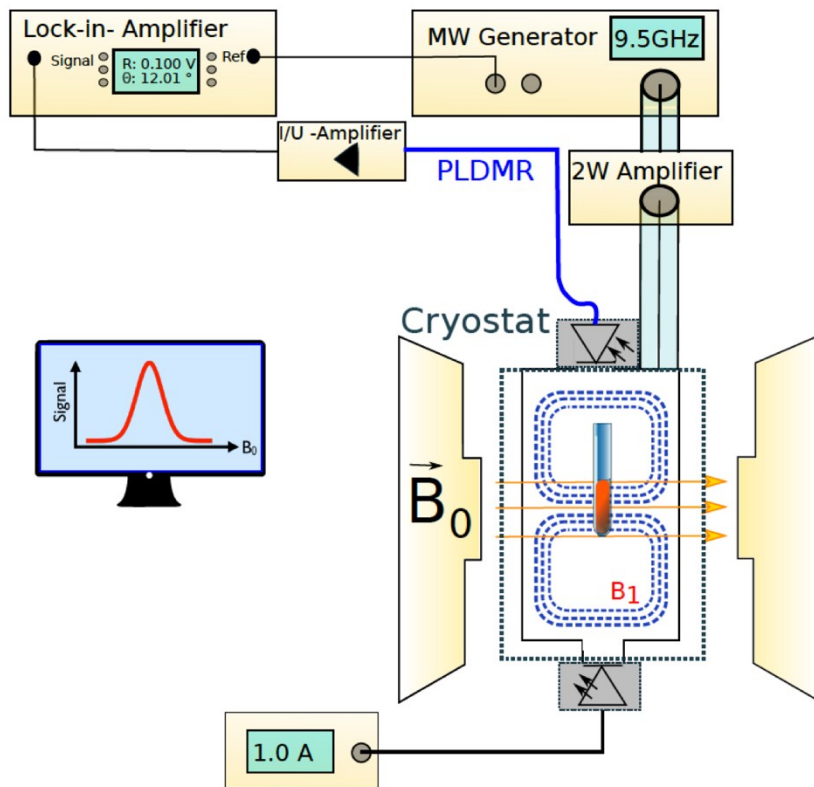
FIG. S14. Scheme of PLDMR setup.
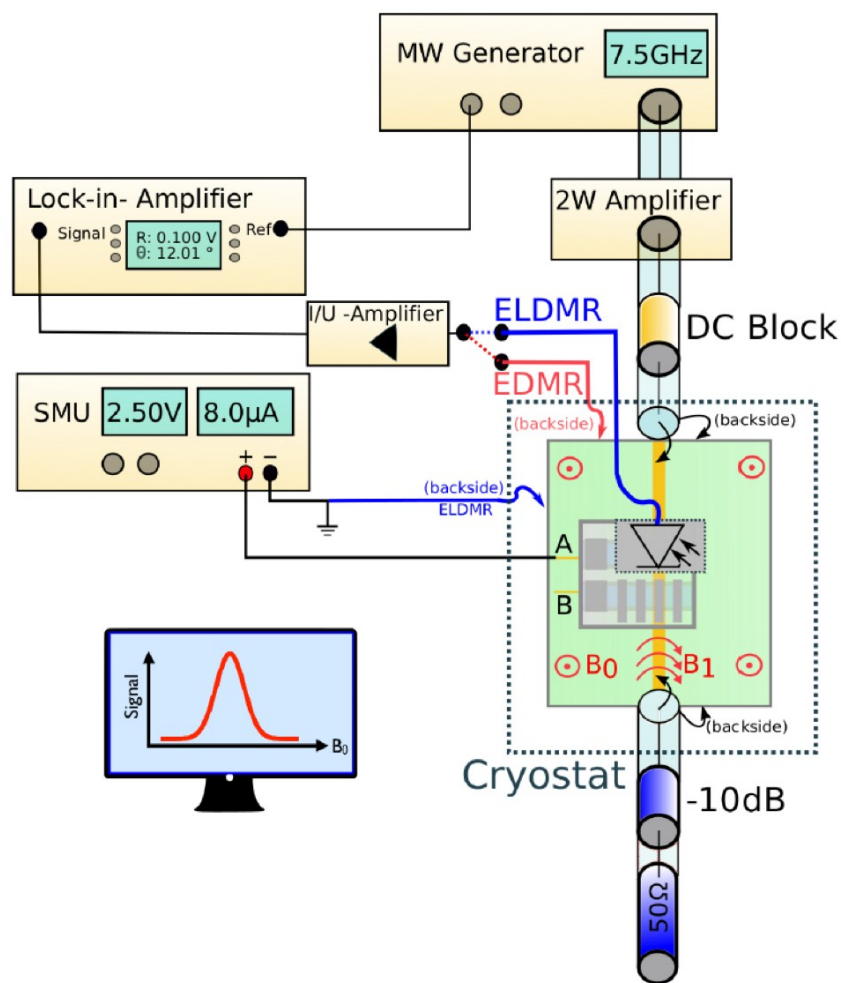
FIG. S15. Scheme of ELDMR setup.

Material	Fabrication	Applied method and figure number in the main manuscript and SI.						
		PL	trPL	PLE	EL	ELDMR	EDMR	PLDMR
m-MTDATA	evaporated	1, S2	2, S2	S1, S2				
	solution processed							S15
3TPYMB	evaporated	1	not excitable[B)]	S1				
	solution processed							S15
BPhen	evaporated	S2, S3		S2, S3				not excitable[A)]
	solution processed							
THCA	evaporated	S3	S3	S3				
	solution processed							no signal
m-MTDATA: 3TPYMB	co-evaporated	1	2	S1	1	3,4,S4, S5,S6,S9	3, S6, S9	S11
	solution processed	S13						4,S4,S9,S11, S13,S15
m-MTDATA: BPhen	co-evaporated	S2	S2	S2	not shown [C)]	S7	not shown [C)]	S11
	solution processed	S13						4,S10,S11,S13
	Bilayer: m-MTDATA from solution, BPhen evaporated on top				S2	4, S7	not shown [C)]	
THCA:BPhen	co-evaporated	S3	S3	S3				
	solution processed							4, S10
	Bilayer: THCA from solution, BPhen evaporated on top				S3	4, S7, S8	S8	
PEDOT:PSS	solution processed						3	

[A)]   BPhen: PLDMR; not excitable with 365 nm UV LED
[B)]   3TPYMB, BPhen: not excitable with 400 nm laser of streak camera setup
[C)]   Identical EL, ELDMR and EDMR spectra for co-evaporated and bilayer OLEDs

TABLE S1. Overview of sample preparation and applied methods.

EQE estimate for m-MTDATA:3TPYMB

A total photoluminescence quantum yield (PLQY) of 0.45 was measured for an oxygen-free m-MTDATA:3TPYMB solid film, whereas the PLQY of the same film fully quenched by oxygen was 0.04. Then the quantum efficiency of the prompt component is $\varphi_{pr} = 0.04$ and of the delayed component is $\varphi_{TADF} = 0.45 - 0.04 = 0.41$. Now, under the assumption that phosphorescence is not present at room temperature, the quantum efficiencies of ISC, RISC, and nonradiative triplet decay can be expressed via φ_{pr} and φ_{TADF}: $\varphi_{ISC} = 1 - \varphi_{pr} = 1 - 0.04 = 0.96$, $\varphi_{RISC} = \varphi_{TADF} = 0.41$, and $\varphi_{nr} = \varphi_{ISC} - \varphi_{TADF} = 0.96 - 0.41 = 0.55$. With that, the maximum internal electroluminescence efficiency of the emitter in an OLED can be expressed as [5]:

$$\Phi_{EL,int} = \eta_S \varphi_{pr} + \eta_S \varphi_{ISC} \varphi_{RISC} + \eta_T \varphi_{RISC};$$

$$\Phi_{EL,int} = 0.25 \cdot 0.04 + 0.25 \cdot 0.96 \cdot 0.41 + 0.75 \cdot 0.41 \approx 0.416;$$

Here η_S and η_T are the portions of singlets and triplets produced via electrical injection (0.25 and 0.75, respectively). We obtained $\Phi_{EL,int} = 41.6\%$, which results in the estimation of $EQE_{max} = 8.3\%$ in devices with an assumed 20% light outcoupling.

References

1   S. Stoll and A. Schweiger, *J. Magn. Reson* 2006, **178**, 1, 42 doi: 10.1016/j.jmr.2005.08.013

2   Q. Huang, S. Zhao, Z. Xu, X. Fan, C. Shen and Q. Yang, *Appl. Phys*. Lett. 2014, **104**, 16, 161112 doi: 10.1063/1.4870492

3   L. Zhu, K. Xu, Y. Wang, J. Chen and D. Ma, *Front. Optoelectron*. 2015, **8**, 4, 439 doi: 10.1007/s12200-015-0492-0

4   V. Cherpak, P. Stakhira, B. Minaev, G. Baryshnikov, E. Stromylo, I. Helzhynskyy, M. Chapran, D. Volyniuk, Z. Hotra, A. Dabuliene, A. Tomkeviciene, L. Voznyak, J. V. Grazulevicius, *ACS Appl. Mater. Interfaces* 2015, **7**, 1219 doi: 10.1021/am507050g

5   A. Endo, K. Sato, K. Yoshimura, T. Kai, A. Kawada, H. Miyazaki, C. Adachi, *Appl. Phys. Lett.* 2011, **98**, 2009–2012 doi: 10.1063/1.124258